Research Article

Multiobjective Synchronous Control of Heavy-Duty Vehicles Based on Longitudinal and Lateral Coupling Dynamics

Yongjie Lu [iD],[1,2] **Tongtong Wang** [iD],[2] **and Hangxing Zhang**[2]

[1]*State Key Laboratory of Mechanical Behavior and System Safety of Traffic Engineering Structures,*
 Shijiazhuang Tiedao University, Shijiazhuang 050043, China
[2]*Shijiazhuang Tiedao University, Shijiazhuang 050043, China*

Correspondence should be addressed to Tongtong Wang; 3512587670@qq.com

The steering system, suspension system, and braking system of the vehicle are interrelated, so the ride comfort and handling stability of the vehicle are also closely related. But the vertical and lateral dynamics equations and controls system of the vehicle are always independent of each other, and the multiobjective control is generally achieved through the coordination of control algorithms. In this paper, taking the dynamic load of the tire as a link, the vertical dynamic model and the lateral dynamic model of heavy-duty vehicle are coupled. When the heavy-duty vehicle is turning, the proposed coupling model not only reflects the influence of the front wheel angle on the vertical motion and the vertical tire load, but also reflects the unevenness of the road surface on vehicle lateral motion. In order to improve the handling stability and transient safety of the vehicle, a synchronous control system combining six-wheel steering and front wheel active steering is proposed. It solves the problem that it is difficult to effectively track the desired yaw rate for the three-axle all-wheel steering vehicle with the middle rear wheel angle as the control input. Under the framework of the vehicle vertical/lateral unified coupling dynamics model, the semiactive suspension system controlled by fuzzy PID and the six-wheel active steering system combined with fuzzy control and fuzzy PID control are integrated. It is verified that the synchronous control method effectively optimizes the vertical and lateral motion characteristics of heavy-duty vehicles during steering and, at the same time, improves the ride comfort and steering stability.

1. Introduction

The current automotive vehicle technology is developing toward a comprehensive Intelligent Vehicles (IVs), and the ultimate goal of IVs is to minimize road traffic accidents. For example, according to the National Highway Traffic Safety Administration (NHTSA), vehicles equipped with Vehicle Stability Control (VSC) can effectively reduce accidents by 35% for sedans and 67% for SUVs compared to vehicles without VSC [1]. IVs will realize intelligent functions by being highly interconnected based on existing Automated Driving Assistance Systems (ADAS) [2, 3].

There are lots of ADAS designed by different suppliers with different technologies and components to accomplish certain control objectives or functions. For example, the active chassis control systems include active suspension system (ASS), electric power steering system (EPS), active four-wheel steering control (4WS), antilock brake system (ABS), and electronic stability program (ESP). These active control systems could improve vehicle handling, stability, ride comfort, etc. Actually, the steering system, suspension system, and braking system of the vehicle are interrelated. So, the ride comfort and handling stability of the vehicle are also closely related (Zhang et al.) [4].

With the rapid development of IVs and vehicle dynamics/tire dynamics, the requirements for the comprehensive performance of the vehicle are getting higher and higher. Especially for a heavy vehicle, when it is in the condition of high-intensity braking/driving, high-speed cornering, and emergency obstacle avoidance, the contact force between the tire and the ground approaches saturation, with strong nonlinearity and uncertain transient

characteristics (Zhang and Li) [5]. Once the heavy-duty vehicle enters the critical zone of instability, the coordinated ride comfort in vertical direction and handling stability control in lateral direction become more complex and important. So, it becomes more and more necessary to improve the ride comfort and handling stability of the vehicle at the same time. The research on vertical/lateral coupling dynamics and control of heavy vehicle is urgently required.

Generally, the research of vehicle ride and handling stability independently adopts vertical and lateral dynamic vehicle models, respectively. For example, in terms of improving vehicle ride comfort, Pazooki et al. [6] studied the establishment of a three-dimensional tire model based on the off-road vehicle dynamics model and analyzed the influence of the vehicle model tires and suspension parameters on the vertical movement. Fan et al. [7] took the vertical acceleration of the seat as the optimization goal and used the artificial fish swarm algorithm to optimize the stiffness and damping of the front suspension of the 1/2 car dynamic model. Ahmadian [8] discussed the applications of magnetorheological (MR) control suspensions for improving ride comfort, handling, and stability in ground vehicles, and he also used the vertical model (semicontrol of 1/4 vehicle). These numerous simulation calculations and experiments have fully proved that the ride comfort of the vehicle can be effectively improved by the active or semiactive control of the vehicle suspension in the vertical direction.

There are also lots of researches in the terms of improving vehicle handling stability. Jiang and Astolfi [9] researched the asymptotic stabilization problem of the lateral controller for autonomous vehicles, based on the lateral vehicle dynamic model.

Guo et al. [10] proposed a real-time nonlinear model predictive control strategy for direct yaw moment control of distributed drive electric vehicles. They also established a supervisory control strategy, which is used for distributed drive electric vehicles to coordinate vehicle handling, lateral stability, and energy economy performance [11]. Norouzi et al. [12] gave a Lyapunov-based robust controller by using a metaheuristic optimization algorithm to control autonomous vehicle lateral performance. Zhang et al. [13] proposed a nonlinear model predictive control (NMPC) strategy to improve vehicle stability and compensate for the random time delay. All-wheel steering of multiaxle vehicles has been widely studied as one of the effective methods to improve the handling stability of multiaxle vehicles. Existing studies have proved that multiaxle all-wheel steering vehicles have better steering flexibility and handling stability than traditional front-wheel steering vehicles (Bu et al.) [14, 15]. For three-axle vehicles, all-wheel steering generally uses the electronically controlled hydraulic power steering system to control the steering of the middle and rear two-axle wheels (Liu et al.) [16, 17]. The advantage of all-wheel steering is that the vehicle's center of mass slip angle can be as close to zero as possible during steering. But the theoretical studies show that the center and rear wheel angles as the only control input cannot effectively track the desired yaw rate well (Wang et al.) [18]. The ultimate goal of the research on

vehicle lateral dynamics is to improve the handling stability of the vehicle, so as to improve the driving safety of the vehicle.

Through the above analysis, we can get a basic conclusion: in order to reduce the difficulty of analysis, these control systems for improving two kinds of performance are usually conducted separately. By establishing independent vertical and lateral dynamic models, the ride comfort and handling stability of the vehicle are studied, respectively. Although it is reasonable to study vehicle dynamics independently in terms of vertical/lateral directions, the actual motion responses in each coordinate direction must be interactive and coupled. The effects of load transfer due to roll and pitch motions are usually ignored when performing stress analyzes on non-spring masses. However, the change of the load will inevitably cause the change of the tire force, thereby affecting the driving trajectory of the vehicle (Sun et al.) [19, 20].

The literature on the optimization analysis of both ride comfort and handling stability is still limited. Some works generally focused on parameters optimization of suspension. Jiang and Wang [21] used Technique for Order Preference by Similarity to Ideal Solution (TOPSIS) method to find the optimal combination of the suspension parameters, with the purpose of improving the vehicle ride comfort and handling stability. Others research design active or semiactive control strategies, such as Chen et al. [22] who proposed semiactive suspension system with MR fluid damper, which can coordinate the body posture angle and reduce the vibration. The results showed that it was suitable for solving the conflict between ride comfort and handing stability. Sun et al. [23] presented an H_∞-linear parameter-varying (LPV) fault-tolerant controller to improve the vehicle vertical and lateral performance in the presence of sensor faults. Fergani et al. [24] also focused on the LPV coordination of suspension and steering/braking vehicle controllers based on the interaction between the vertical and lateral behaviors of the vehicle. Zhao et al. [25] proposed a hierarchical control system considering the longitudinal, lateral, and vertical dynamic performance for distributed Electric Vehicle (EV) based on integrated control theory. Kwon et al. [26] performed a multiobjective optimization of the HPS design, and a Pareto front considering the contradiction between the comfort and stability of the performances is obtained. These important studies provide great ideas for us to improve the comprehensive performance of intelligent vehicles. At present, the vertical and lateral dynamics equations and controls are always independent of each other, and the multiobjective control of the vehicle is achieved through the coordination of control algorithms. But there is a lack of research on a unified vehicle dynamics equation for the coupling of vertical and lateral dynamics, especially for heavy-duty vehicle.

In order to simultaneously improve heavy-duty vehicle lateral stability and vertical ride comfort performance together, a three-dimension vertical/lateral coupling dynamic and control model is proposed. The contributions of this paper are as follows: (1) a research framework for coupling vertical and lateral dynamics of heavy-duty vehicles is proposed. When the heavy-duty vehicle is driving, especially

in the turning condition, the proposed coupling dynamic model not only reflects the influence of the front wheel angle on the vertical motion of the vehicle and the vertical load of the tire, but also reflects the unevenness of the road surface on vehicle lateral motion. (2) Based on the combination of all-wheel steering control and active front-wheel control, a six-wheel active steering control idea is proposed and applied in the vertical/side coupling model. It solves the problem that it is difficult to effectively track the desired yaw rate for the three-axle all-wheel steering vehicle with the middle rear wheel angle as the control input.

The structure of this article is as follows: in Section 2, vertical-lateral coupling dynamics control model for heavy-duty vehicles is given, and a six-wheel active steering control system is proposed. In Section 3, integrated control strategies of ride comfort and steering stability are given. In Section 4, some simulations are done to explain the different dynamic response of coupling and uncoupling models, control effect on ride comfort, and handling stability with coupled model. Finally, in Section 5, we summarize the above contents and put forward the future research direction.

2. Vertical-Lateral Coupling Dynamics Control Model for Heavy-Duty Vehicles

2.1. Basic Idea of Vehicle Vertical/Lateral Coupling Dynamics Model. In order to simultaneously improve the ride comfort and steering stability of the vehicle, the three-dimension vertical/lateral coupling dynamics model for vehicle system is proposed. The coupled dynamics model is divided into a *vertical dynamics* module, a *tire* module, a *lateral dynamics* module, and an *external input* module (including random excitation on uneven roads and the steering angle of the front wheels operated by the driver). The roll of the vehicle motion belongs to both the vertical and lateral dynamics modules of the vehicle. The interrelationship among the modules of the coupling model is shown in Figure 1.

As can be seen from Figure 1, when the vehicle is in steering motion (lateral motion), the principle of the three-dimensional vertical/lateral coupling model is as follows:

(1) Taking the dynamic load of the tire as a link, the vertical dynamic model and the lateral dynamic model of the vehicle are coupled through the vertical motion of the tire module and the rolling motion of the vehicle body.

(2) When the lateral dynamics model is input by the front wheel angle, the yaw rate, acceleration of yaw angle, and lateral acceleration generated by the vehicle will affect the rolling motion of the vertical dynamics model.

(3) Similarly, when the vertical dynamics model is input by road roughness, the roll angle acceleration in the roll motion will also affect the yaw motion and lateral motion of the lateral dynamics model. At the same time, the rolling motion of the car body will also affect the vertical motion and pitching motion in the vertical dynamics module.

In short, the unified coupling dynamic model proposed in this paper realizes that the vertical dynamic model and the lateral dynamic model are interrelated and inseparable when the vehicle is driving, which is more suitable for the turning condition. This provides a theoretical basis for the synchronous control of vehicle ride comfort and handling stability later.

2.2. Three-Dimensional Vehicle Dynamic Model with Semiactive Suspension. A vertical-lateral coupling model of vehicle is established, including vehicle vertical motion, pitch motion, roll motion, lateral motion, yaw motion, vertical motion of front tires, and vertical and pitch motion of balance suspension rods on mid-rear axle. In order to improve the smoothness of the coupled model, a semiactive suspension control system is adopted for the vehicle model. The vertical/lateral coupling dynamics model of the vehicle based on the semiactive suspension system is shown in Figure 2.

In Figure 2, m_b is the mass of the vehicle's body; m_{tlf}, m_{tlm} and m_{tlr} are the masses of the front, middle, and rear wheels of the left side of the vehicle; m_{trf}, m_{trm} and m_{trr} are the masses of the front, middle, and rear wheels of the right side of the vehicle; m_{lm} and m_{rp} are the masses of the left and right suspension balance rods; k_{slf} and k_{srf} are the left and right stiffness of leaf springs of front suspension; c_{slf} and c_{srf} are the left and right damping of the shock absorbers of the front suspension; k_{slr} and k_{srr} are the left and right stiffness of leaf springs of balanced suspension; c_{slr} and c_{srr} are the left and right damping of the shock absorbers of the balanced suspension; k_{tlf} and k_{trf} are the left and right stiffness of front tires; k_{tlm} and k_{trm} are the left and right stiffness of middle tires; k_{tlr} and k_{trr} are the left and right stiffness of rear tires; f_{si} ($i = lf$, lr, rf, rr) are the control force of the damping coefficient of the semiactive suspension system; q_i ($i = 1, 2, 3, 4, 5, 6$) are the road excitation; I_{by} and I_{bx} are the pitch and roll moments of inertia of the vehicle body; I_{lpy} and I_{rpy} are the left and right pitch moments of inertia of balanced suspension robs; l_1 is the distance from the front axle to mass center; l_2 is the distance from the center of the suspension to the center of mass of the vehicle; l_3 is the distance from the middle axle to the rear axle; b_1 and b_2 are the distance from the left and right suspension to the mass center; v_x is the longitudinal speed of vehicle; v_y is the lateral speed of vehicle; α_{fl}, α_{ml} and α_{rl} are side-slip angles of the left side of front, middle, and rear tires; α_{fr}, α_{mr} and α_{rr} are side-slip angles of the right side of front, middle, and rear tire; F_{yfl}, F_{yml} and F_{yrl} are lateral forces of the left side of front, middle, and rear tires; F_{yfr}, F_{ymr} and F_{yrr} are lateral forces of the right side of front, middle, and rear tires; δ_f the cornering angle of front tire; h is rolling moment arm.

2.3. Active Steering Control of Six Wheels. For the three-axle heavy-duty vehicle, the so-called six-wheel active steering control is a combination of all-wheel steering control and active front-wheel steering control. All-wheel steering is one of the effective methods to improve the steering stability of multiaxle vehicles. It is proven that the multiaxle vehicles
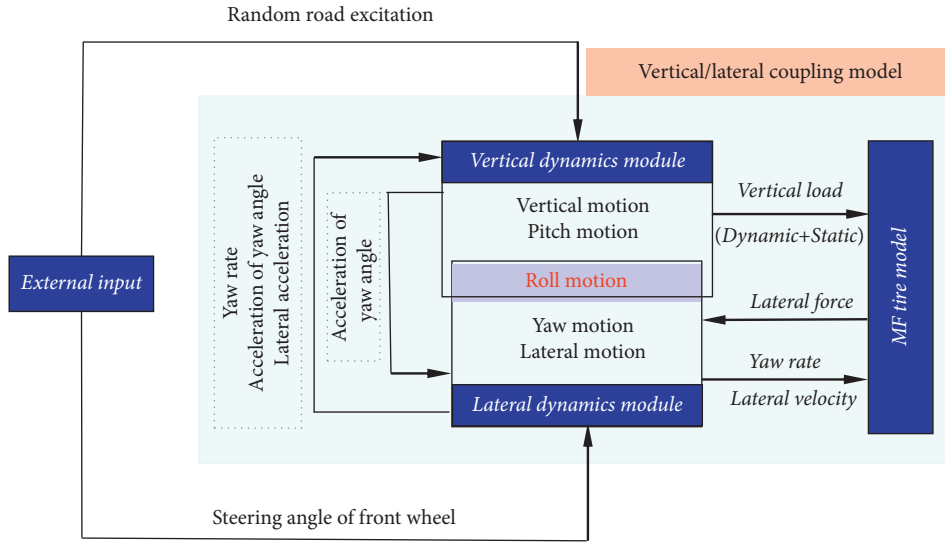
FIGURE 1: Structure of vertical/lateral coupling dynamics model of heavy vehicle.
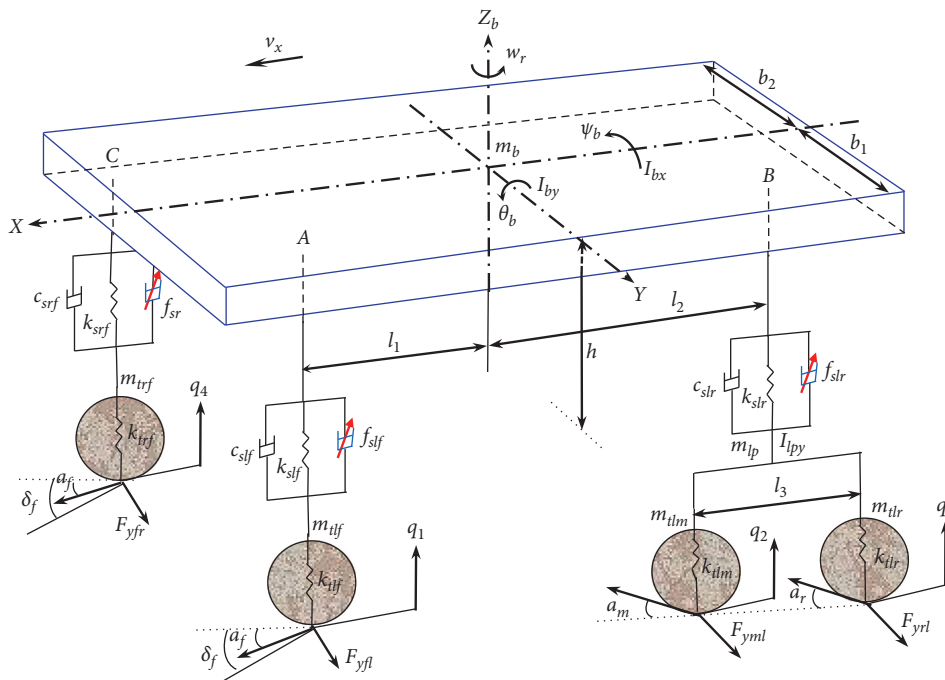

FIGURE 2: Vertical/lateral coupling dynamics model of heavy-duty vehicle with semiactive suspension.

with all-wheel steering have better steering flexibility and steering stability than conventional front-wheel steering vehicles (Huh et al.) [27]. Based on the coupled heavy-duty vehicle model and semiactive suspension system, a six-wheel active steering control system is proposed to improve the steering stability of the vehicle in this section.

The advantage of all-wheel steering is that the side-slip angle of the vehicle can be as close as possible to zero when steering. Studies have shown that the desired yaw rate can not be effectively tracked only by the middle and rear wheel

angles as control inputs (Chen et al.) [28]. According to these research conclusions, an active front-wheel steering model has been added based on all-wheel steering. The structure detail of active front-wheel steering can be found in reference [29]. Active front wheel steering can make the steering angle of the front wheels larger or smaller than the steering angle given by the driver to the front wheels through the steering wheel, and the steering angle is corrected according to the driving conditions of the vehicle [30]. Taking advantage of this feature of active front wheel

steering, this paper uses the additional angle generated by active front wheel steering as input to control the yaw rate of the vehicle. In order to make the vehicle have a more ideal center of mass slip angle and yaw rate when turning, and to better improve the steering stability of the vehicle, this paper proposes the combination control system of six-wheel all-wheel steering and front wheel active steering. The schematic diagram of the active steering control system is shown in Figure 3.

In Figure 3, w_r is the yaw rate; β is the side-slip angle of vehicle; δ_f is the front wheel steering angle generated by the driver input; $\Delta\delta_f$ is the front wheel additional angle generated by the front wheel active steering; δ_m is the middle wheel steering Rotation angle; δ_r is the rear wheel angle of all-wheel steering; B is the distance between the left and right suspension, $B = b_1 + b_2$; a_1, a_2 and a_3 are the distances from the front, middle, and rear axles to the vehicle center of mass, respectively.

2.4. Vertical/Lateral Coupling Dynamics Control Model of Heavy Vehicle.

Based on the semiactive suspension system and the six-wheel active steering system described above, the vertical/lateral coupling dynamics model of the three-axle heavy-duty vehicle is established. According to the D'Alembert principle, the differential equations for the vertical/lateral coupling dynamics model of a three-axle heavy-duty vehicle with a six-wheel active steering system are shown as follows:

The vertical motion equation of the vehicle body:

$$
\begin{aligned}
m_b \ddot{z}_b = &-\left[k_{\text{slf}}\left(z_b - \theta_b l_2 - z_{\text{tlf}}\right) + c_{\text{slf}}\left(\dot{z}_b - \dot{\theta}_b l_2 - \dot{z}_{\text{tlf}}\right)\right] \\
&-\left[k_{\text{slr}}\left(z_b + \theta_b l_2 - z_{lp}\right) + c_{\text{slr}}\left(\dot{z}_b + \dot{\theta}_b l_2 - \dot{z}_{lp}\right)\right] \\
&-\left[k_{\text{srf}}\left(z_b - \theta_b l_1 - z_{\text{trf}}\right) + c_{\text{srf}}\left(\dot{z}_b - \dot{\theta}_b l_1 - \dot{z}_{\text{trf}}\right)\right] \\
&-\left[k_{\text{srr}}\left(z_b + \theta_b l_2 - z_{rp}\right) + c_{\text{srr}}\left(\dot{z}_b + \dot{\theta}_b l_2 - \dot{z}_{rp}\right)\right] \\
&-f_{\text{slf}} - f_{\text{slr}} - f_{\text{srf}} - f_{\text{srr}}.
\end{aligned} \tag{1}
$$

The pitch motion equation of the vehicle body:

$$
\begin{aligned}
I_{by} \ddot{\theta}_b = &\, l_1 \left[k_{\text{slf}}\left(z_b - \theta_b l_2 - z_{\text{tlf}}\right) + c_{\text{slf}}\left(\dot{z}_b - \dot{\theta}_b l_2 - \dot{z}_{\text{tlf}}\right)\right] \\
&- l_2 \left[k_{\text{slr}}\left(z_b + \theta_b l_2 - z_{lp}\right) + c_{\text{slr}}\left(\dot{z}_b + \dot{\theta}_b l_2 - \dot{z}_{lp}\right)\right] \\
&+ l_1 \left[k_{\text{srf}}\left(z_b - \theta_b l_1 - z_{\text{trf}}\right) + c_{\text{srf}}\left(\dot{z}_b - \dot{\theta}_b l_1 - \dot{z}_{\text{trf}}\right)\right] \\
&- l_2 \left[k_{\text{srr}}\left(z_b + \theta_b l_2 - z_{rp}\right) + c_{\text{srr}}\left(\dot{z}_b + \dot{\theta}_b l_2 - \dot{z}_{rp}\right)\right] \\
&+ l_1 f_{\text{slf}} - l_2 f_{\text{slr}} + l_1 f_{\text{srf}} - l_2 f_{\text{srr}}.
\end{aligned} \tag{2}
$$

The roll motion equation of the vehicle body:

$$
\begin{aligned}
\left(I_x + m_b h^2\right)\ddot{\psi}_b + I_{xz}\dot{w}_r = &\, m_b h\left(\dot{v}_y + v_x w_r\right) \\
&-\left(c_{of} + c_{or}\right)\dot{\psi}_b \\
&-\left(k_{of} + k_{or}\right)\psi \\
&- b\left(k_{\text{slf}} z_{\text{tlf}} + c_{\text{slf}} \dot{z}_{\text{tlf}}\right) \\
&- b\left(k_{\text{slr}} z_{lp} + c_{\text{slr}} \dot{z}_{lp}\right) \\
&+ b_2\left(k_{\text{srf}} z_{\text{trf}} + c_{\text{srf}} \dot{z}_{\text{trf}}\right) \\
&+ b_2\left(k_{\text{srr}} z_{rp} + c_{\text{srr}} \dot{z}_{rp}\right) \\
&+ k_{\text{slf}} b_1 \left(\theta_b l_1\right) - k_{\text{srf}} b_2 \left(\theta_b l_1\right) \\
&- k_{\text{slr}} b_1 \left(\theta_b l_2\right) + k_{\text{srr}} b_2 \left(\theta_b l_2\right) \\
&+ c_{\text{slf}} b_1 \left(\dot{\theta}_b l_1\right) - c_{\text{srf}} b_2 \left(\dot{\theta}_b l_1\right) \\
&- c_{\text{slr}} b_1 \left(\dot{\theta}_b l_2\right) + k_{\text{srr}} b_2 \left(\dot{\theta}_b l_2\right) \\
&- b_1 f_{\text{slf}} - b_1 f_{\text{slr}} + b_2 f_{\text{srf}} + b_2 f_{\text{srr}}.
\end{aligned} \tag{3}
$$

The vertical motion equations of the left and right tires of the front suspension:

$$
\begin{aligned}
m_{\text{tlf}} \ddot{z}_{\text{tlf}} = &\, k_{\text{slf}} \left(z_b - \theta_b l_1 + \psi_b b_1 - z_{\text{tlf}}\right) \\
&+ c_{\text{slf}} \left(\dot{z}_b - \dot{\theta}_b l_1 + \dot{\psi}_b b_1 - \dot{z}_{\text{tlf}}\right) \\
&- k_{\text{tlf}} \left(z_{\text{tlf}} - q_1\right) + f_{\text{slf}}, \\
m_{\text{trf}} \ddot{z}_{\text{trf}} = &\, k_{\text{srf}} \left(z_b - \theta_b l_1 - \psi_b b_2 - z_{\text{trf}}\right) \\
&+ c_{\text{srf}} \left(\dot{z}_b - \dot{\theta}_b l_1 - \dot{\psi}_b b_2 - \dot{z}_{\text{trf}}\right) \\
&- k_{\text{trf}} \left(z_{\text{trf}} - q_4\right) + f_{\text{srf}}.
\end{aligned} \tag{4}
$$

The vertical motion equations of the left and right tires of the balanced suspension:

$$
\begin{aligned}
\left(m_{lp} + m_{\text{tlr}} + m_{\text{tlm}}\right)\ddot{z}_{lp} = &\, k_{\text{slr}}\left(z_b + \theta_b l_2 + \psi_b b_1 - z_{lp}\right) \\
&+ c_{\text{slf}}\left(\dot{z}_b + \dot{\theta}_b l_2 + \dot{\psi}_b b_1 - \dot{z}_{lp}\right) \\
&- k_{\text{tlm}}\left(z_{\text{tlm}} - q_2\right) - k_{\text{tlm}}\left(z_{\text{tlr}} - q_3\right), \\
\left(m_{rp} + m_{\text{trr}} + m_{\text{trm}}\right)\ddot{z}_{rp} = &\, k_{\text{slr}}\left(z_b + \theta_b l_2 + \psi_b b_2 - z_{rp}\right) \\
&+ c_{\text{srr}}\left(\dot{z}_b + \dot{\theta}_b l_2 + \dot{\psi}_b b_2 - \dot{z}_{rp}\right) \\
&- k_{\text{trm}}\left(z_{\text{trm}} - q_5\right) - k_{\text{tlm}}\left(z_{\text{tlr}} - q_6\right).
\end{aligned} \tag{5}
$$

The pitch motion equations of the left and right tires of the balanced suspension:

$$\left(\frac{I_{\text{lpy}} + m_{\text{tlm}}l_3^2}{4} + \frac{m_{\text{tlm}}l_3^2}{4}\right)\ddot{\theta}_{lp} = \frac{k_{\text{tlm}}\left(z_{lp} - l_3\theta_{lp}/2 - q_2\right)l_3}{2}$$

$$+ \frac{k_{\text{tlr}}\left(z_{lp} + l_3\theta_{lp}/2 - q_3\right)l_3}{2},$$

$$\left(\frac{I_{\text{rpy}} + m_{\text{trm}}l_3^2}{4} + \frac{m_{\text{trm}}l_3^2}{4}\right)\ddot{\theta}_{rp} = \frac{k_{\text{trm}}\left(z_{rp} - l_3\theta_{rp}/2 - q_5\right)l_3}{2}$$

$$+ \frac{k_{\text{trr}}\left(z_{rp} + l_3\theta_{rp}/2 - q_6\right)l_3}{2}.$$

(6)

The lateral motion equation of the vehicle:

$$m\left(\dot{v}_y - v_x w_r\right) - m_b h\ddot{\psi} = \left(F_{\text{yfl}} + F_{\text{yfr}}\right)\cos\left(\delta_f + \Delta\delta\right)$$
$$+ \left(F_{\text{yml}} + F_{\text{ymr}}\right)\cos\delta_m + \left(F_{\text{yrl}} + F_{\text{yrr}}\right)\cos\delta_r.$$

(7)

The yaw motion equation of the vehicle:

$$I_\zeta\dot{\omega}_\rho + I_{\xi\zeta}\ddot{\psi} = \alpha_1\left(\Phi_{\psi\varphi\lambda} + \Phi_{\psi\varphi\rho}\right)\chi o\sigma\left(\delta_\varphi + \Delta\delta\right)$$

$$+ \frac{B}{2}\left(\Phi_{\psi\varphi\lambda} - \Phi_{\psi\varphi\rho}\right)\sigma\iota\nu\left(\delta_\varphi + \Delta\delta\right)$$

$$- \alpha_2\left(\Phi_{\psi\mu\lambda} + \Phi_{\psi\mu\rho}\right)\chi o\sigma\delta_\mu + \frac{B}{2}\left(\Phi_{\psi\mu\lambda} - \Phi_{\psi\mu\rho}\right)\sigma\iota\nu\delta_\mu$$

$$- \alpha_3\left(\Phi_{\psi\rho\lambda} + \Phi_{\psi\rho\rho}\right)\chi o\sigma\delta_\rho + \frac{B}{2}\left(\Phi_{\psi\rho\rho} - \Phi_{\psi\rho\lambda}\right)\sigma\iota\nu\delta_\rho.$$

(8)

2.5. Magic Formula Tire Model and Dynamical Vertical Loading. The Magic Formula (MF) tire model is one of the semiempirical models. It can be used to describe the basic physical and structural characteristics of the tire well, with high precision, and the simulation results are extremely close to the actual tire test results [31]. Therefore, the lateral force of the tire in the lateral dynamic equation is solved by a nonlinear MF tire model to get closer to the actual tire model. MF tire model was provided by H. B. Pacejka. The model can fully express the working conditions of longitudinal force, lateral force, and positive moment with only one set of the same formula.

In this paper, it is assumed that the longitudinal speed of the vehicle is constant, so the vehicle is operated under a single condition of pure turning during the steering calculation. The formula for calculating the lateral force under the pure turning condition is obtained by the general form of MF model:

$$F_y = D_y\sin\left\{C_y\arctan\left[B_y x - E_y\left(B_y x - \arctan\left(B_y x\right)\right)\right]\right\} + S_v,$$

(9)

where $C_y = 1.3$; $x = \alpha + S_h$; $D_y = a_1 F_z^2 + a_1 F_z$; $B_y C_y D_y = a_3\sin\left[a_4\arctan\left(a_5 F_z\right)\right]\left(1 - a_{12}|\gamma|\right)$; $B_y = \left(B_y C_y D_y\middle/\right.$ $\left(C_y\right.$

$\left.D_y\right)\right)$; $E_y = a_6 F_z^2 + a_7 F_z + a_8$; $S_h = a_9\gamma$; $S_v = \left(a_{10}F_z^2 + a_{11}F_z\right)\gamma$; α is the side-slip angle of tire, F_z is the vertical loading of tire, and γ is the camber angle of tire. $a_1, \ldots, a_{12}$ are the fitting parameters. The values of reference [31] are shown in Table 1.

The solution of the side-slip angle of each tire is shown in the following equation:

$$\begin{cases} a_{fl} = \arctan\left(\dfrac{v_y + a_1 w_r}{v_x}\right) - \left(\delta_f - \Delta\delta\right), \\[2mm] a_{fr} = \arctan\left(\dfrac{v_y + a_1 w_r}{v_x}\right) - \left(\delta_f - \Delta\delta\right), \\[2mm] a_{ml} = \arctan\left(\dfrac{v_y + a_2 w_r}{v_x}\right) - \delta_m, \\[2mm] a_{mr} = \arctan\left(\dfrac{v_y + a_2 w_r}{v_x}\right) - \delta_m, \\[2mm] a_{rl} = \arctan\left(\dfrac{v_y + a_3 w_r}{v_x}\right) - \delta_r, \\[2mm] a_{rr} = \arctan\left(\dfrac{v_y + a_3 w_r}{v_x}\right) - \delta_r. \end{cases}$$

(10)

The vertical load of the left and right tires of the vehicle is basically equal when traveling in a straight line. Actually, the vertical loads of two sides tires are different due to the roll moment during steering, which affects the lateral deflection characteristics of the tire. Considering the redistribution of the vertical loads on the left and right tires, the dynamical vertical loads of each tire when the vehicle is steering are expressed as follows:

$$\begin{cases} F_{zfl} = \dfrac{d}{2L}m_b g + m_{tfl}g - \dfrac{m_s g a_y dH}{2LB} - \dfrac{m_{trl}g a_y h_{\mu l}}{B} - \dfrac{K_{of}\psi_b}{B}, \\[3mm] F_{zfr} = \dfrac{d}{2L}m_b g + m_{tfr}g - \dfrac{m_s g a_y dH}{2LB} + \dfrac{m_{tfr}g a_y h_{\mu l}}{B} + \dfrac{K_{of}\psi_b}{B}, \\[3mm] F_{zml} = \dfrac{a_1}{4L}m_b g + m_{tml}g - \dfrac{m_s g a_y dH}{8LB} - \dfrac{m_{tml}g a_y h_{\mu 2}}{2B} - \dfrac{K_{or}\psi_b}{2B}, \\[3mm] F_{zmr} = \dfrac{a_1}{4L}m_b g + m_{tmr}g + \dfrac{m_s g a_y dH}{8LB} + \dfrac{m_{tmr}g a_y h_{\mu 2}}{2B} + \dfrac{K_{or}\psi_b}{2B}, \\[3mm] F_{zrl} = \dfrac{a_1}{4L}m_b g + m_{trl}g - \dfrac{m_s g a_y dH}{8LB} - \dfrac{m_{trl}g a_y h_{\mu 3}}{2B} - \dfrac{K_{or}\psi_b}{2B}, \\[3mm] F_{zrr} = \dfrac{a_1}{4L}m_b g + m_{trr}g + \dfrac{m_s g a_y dH}{8LB} + \dfrac{m_{trr}g a_y h_{\mu 3}}{2B} + \dfrac{K_{or}\psi_b}{2B}. \end{cases}$$
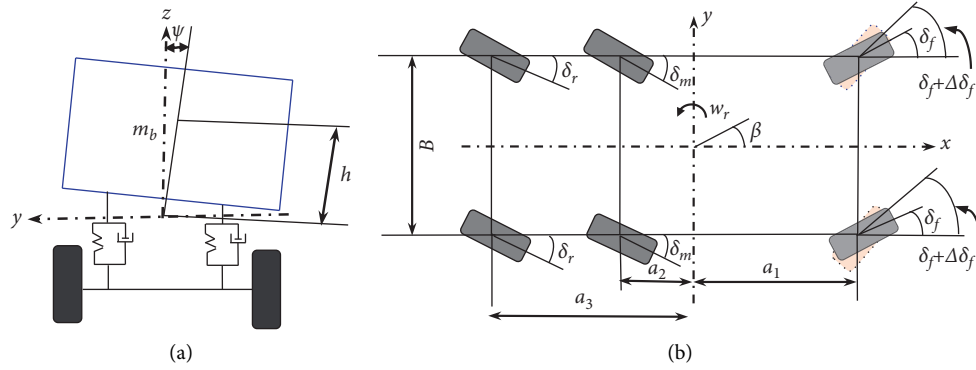
(11)

FIGURE 3: Schematic diagram of six-wheel active steering system. (a) Rear view of vehicle model. (b) Top view of vehicle model.

TABLE 1: Fitting parameter values of MF tire model.

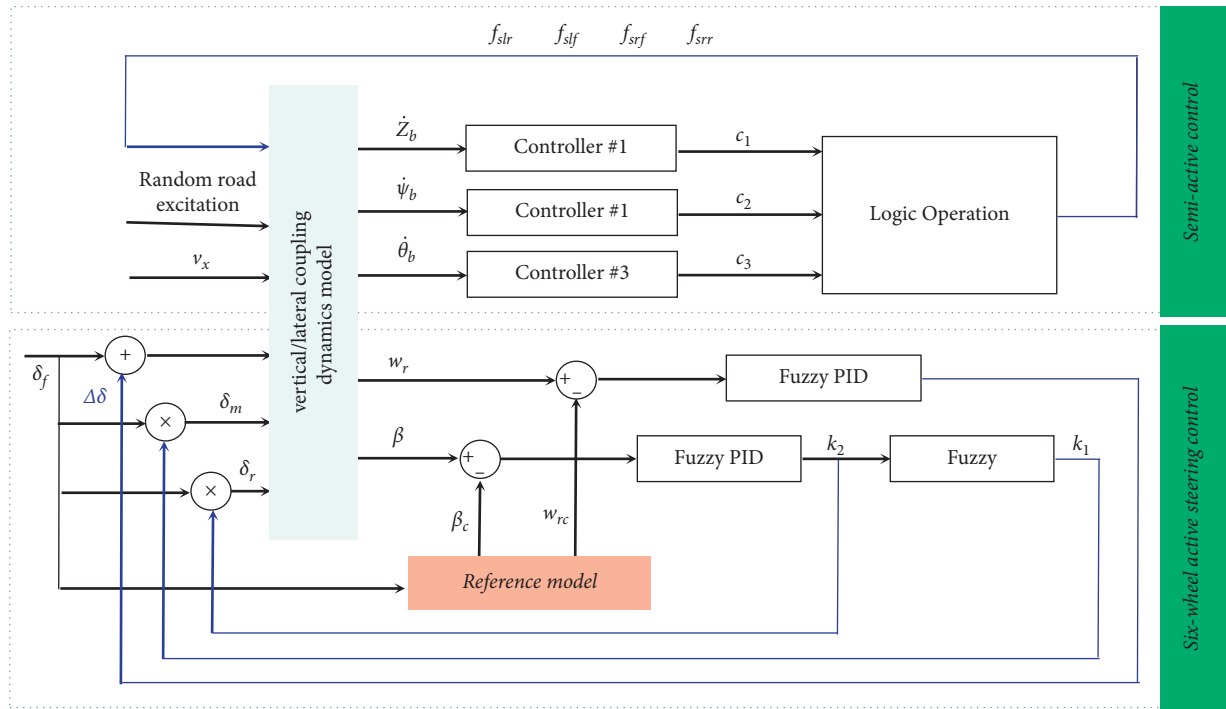| a_1	a_2	a_3	a_4	a_5	a_6
−22.1	1011	1078	1.82	0.208	0
a_7	a_8	a_9	a_{10}	a_{11}	a_{12}
−0.354	0.707	0.028	0	14.8	0.022

FIGURE 4: Simulation model of vehicle ride comfort and steering stability synchronous control.

3. Integrated Control Strategy of Ride Comfort and Steering Stability

The ultimate purpose of studying the vertical-lateral coupling dynamics of the vehicle is to comprehensively improve the ride comfort and handling stability of the vehicle.

Through the establishment and simulation of the vehicle's vertical-lateral coupling dynamics model above, it is known that the vehicle's ride comfort and handling stability are interrelated and inseparable during steering. To simultaneously improve its ride comfort and handling stability is difficult to achieve with a single control method. In order to

TABLE 2: Fuzzy control rule of proportional coefficient k_2.

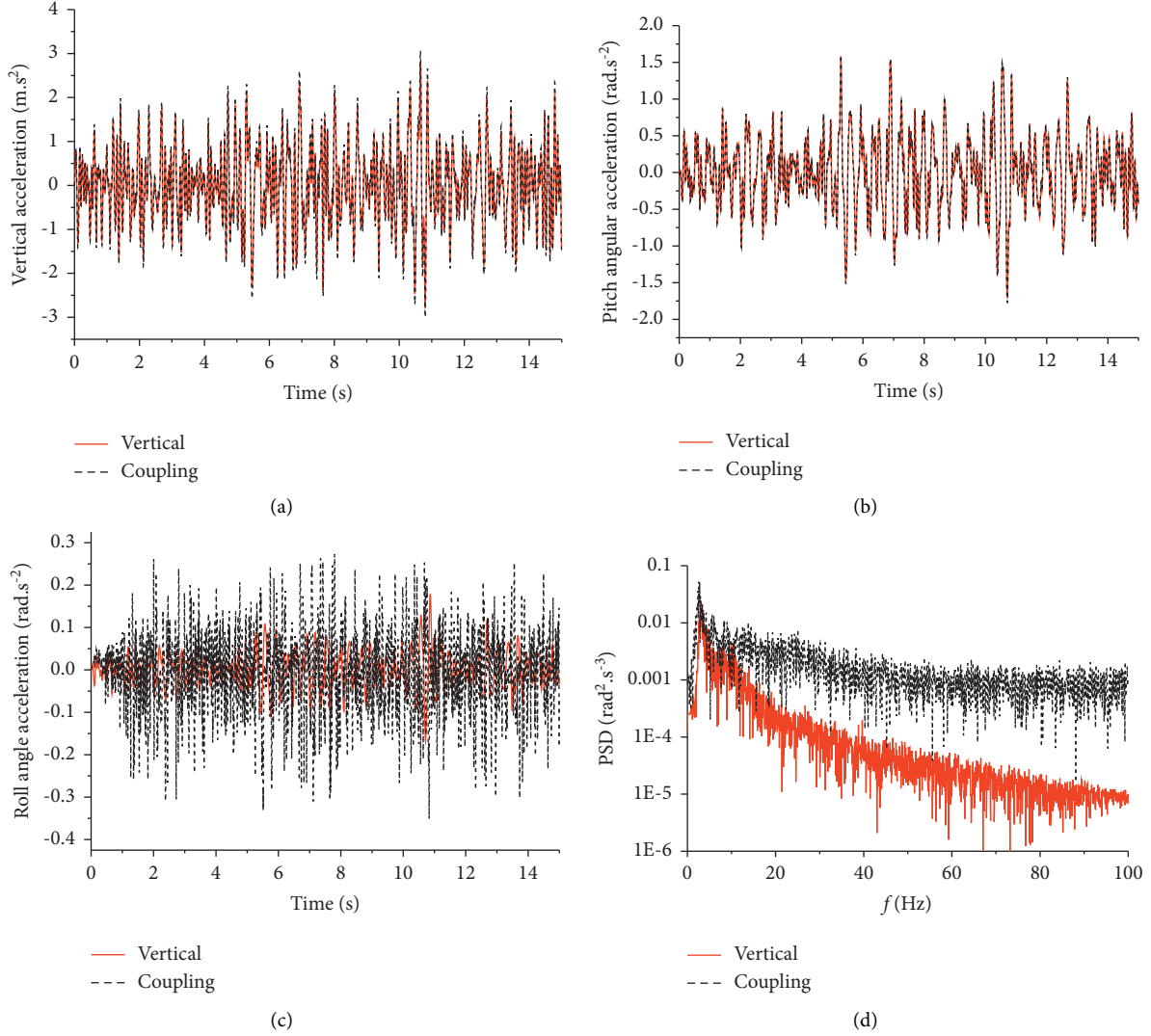| k_2	NB	NM	NS	ZE	PS	PM	PB
k_1	NM	NS	NS	ZE	PM	PB	PB

(a)

(b)

(c)

(d)

FIGURE 5: Ride comfort response (angular step condition, B-level random road). (a) Vertical acceleration of vehicle. (b) Car body pitching angular acceleration. (c) Roll angle acceleration time domain. (d) Roll angle acceleration frequency domain.

improve the ride comfort and handling stability of the vehicle model at the same time, this section will combine semiactive suspension control with six-wheel active steering control. The control strategy block diagram is shown in Figure 4. Three fuzzy controllers are designed for the semiactive suspension system, and the fuzzy controller and fuzzy PID controller are designed for the six-wheel active steering system, respectively.

3.1. Ideal Reference Model for Six-Wheel Active Steering. The purpose of establishing an ideal reference model for a vehicle is primarily to improve the vehicle's ability to maintain a safe trajectory and the vehicle's steering flexibility. The above two indicators can be achieved by controlling the vehicle side-slip angle and the yaw rate respectively [15]. Therefore, the ideal yaw rate and the ideal centroid angle are used as the tracking state variables of the
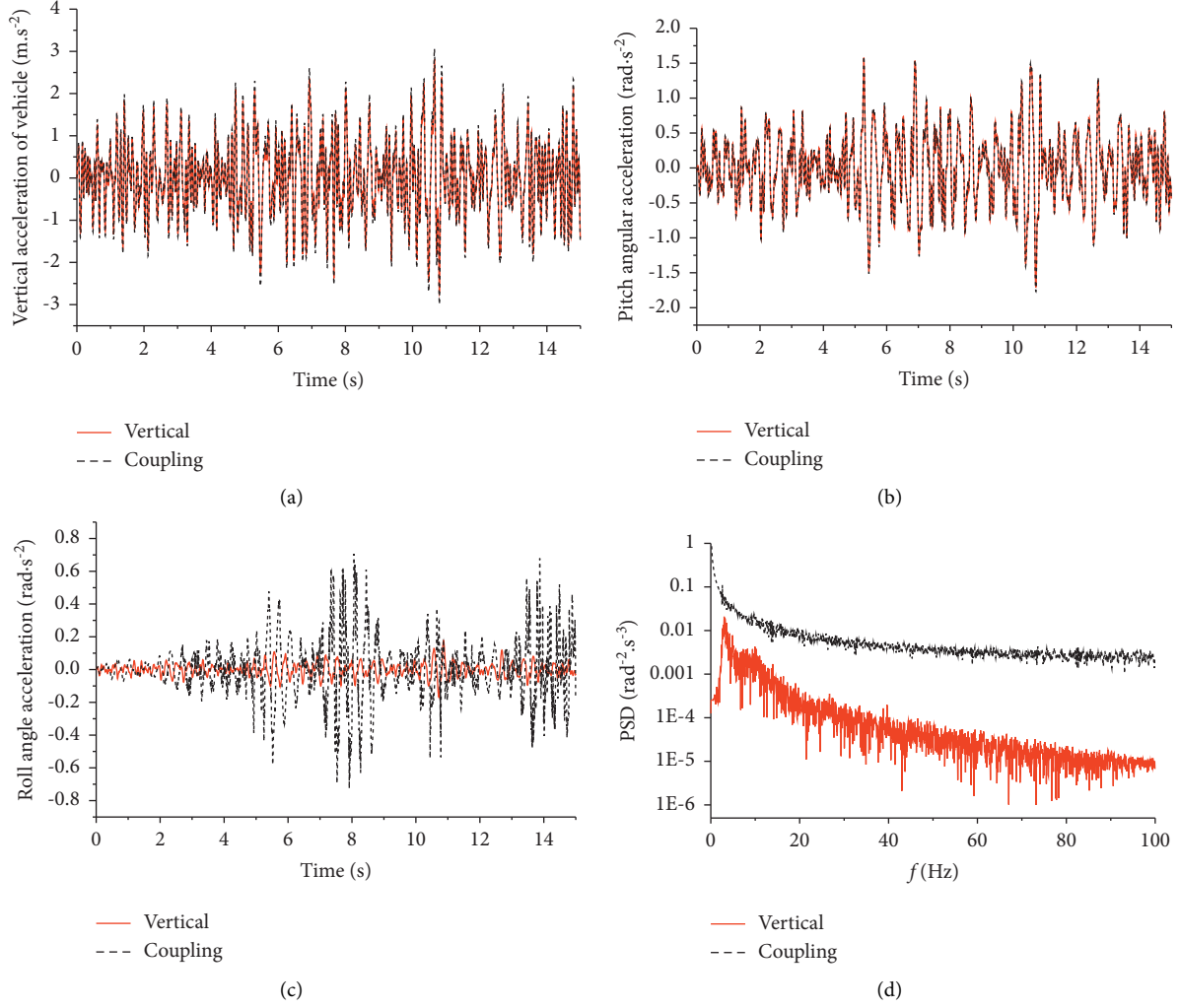
FIGURE 6: Ride comfort response (serpentine working condition, B-level random road). (a) Vertical acceleration of vehicle. (b) Pitching angular acceleration. (c) Roll angle acceleration time domain. (d) Roll angle acceleration frequency domain.

control system. A linear two-degree-of-freedom lateral dynamics model is generally used as a reference model, which has ideal steering characteristics [32], The motion equation is expressed as

$$\begin{cases} \dot{\beta}_c = \left[\dfrac{\left(2k_{cf}a_f + 2k_{cm}a_m + 2k_{cr}a_r\right)}{(mv_x)} \right] - w_r, \\[2em] \dot{w}_{rc} = \left[\dfrac{\left(2a_1 k_{cf}a_f - 2a_2 k_{cn}a_m - 2a_3 k_{cr}a_r\right)}{I_z} \right], \end{cases} \quad (12)$$

where k_{cf}, k_{cm} and k_{cr} are the cornering stiffness of the front, middle, and rear wheels; α_f, α_m and α_r are the side-slip angles of the front, middle, and rear axle tires, and the expression is shown as follows:

$$\begin{cases} \alpha_f = \beta_c + \left(\dfrac{a_1}{v_x}\right) w_{rc} - \delta_f, \\[1.5em] \alpha_m = \beta_c - \left(\dfrac{a_2}{v_x}\right) w_{rc}, \\[1.5em] \alpha_r = \beta_c + \left(\dfrac{a_3}{v_x}\right) w_{rc}. \end{cases} \quad (13)$$

When the ideal vehicle model is being steering, it should be ensured that the vehicle does not slip. Then, the side-slip angle value ideal model of the vehicle should be zero, $\beta_c = 0$. At the same time, the yaw rate is quickly stabilized by the first-order inertial transfer function characteristic [33]. Equation (13) is substituted into the equation (15) according
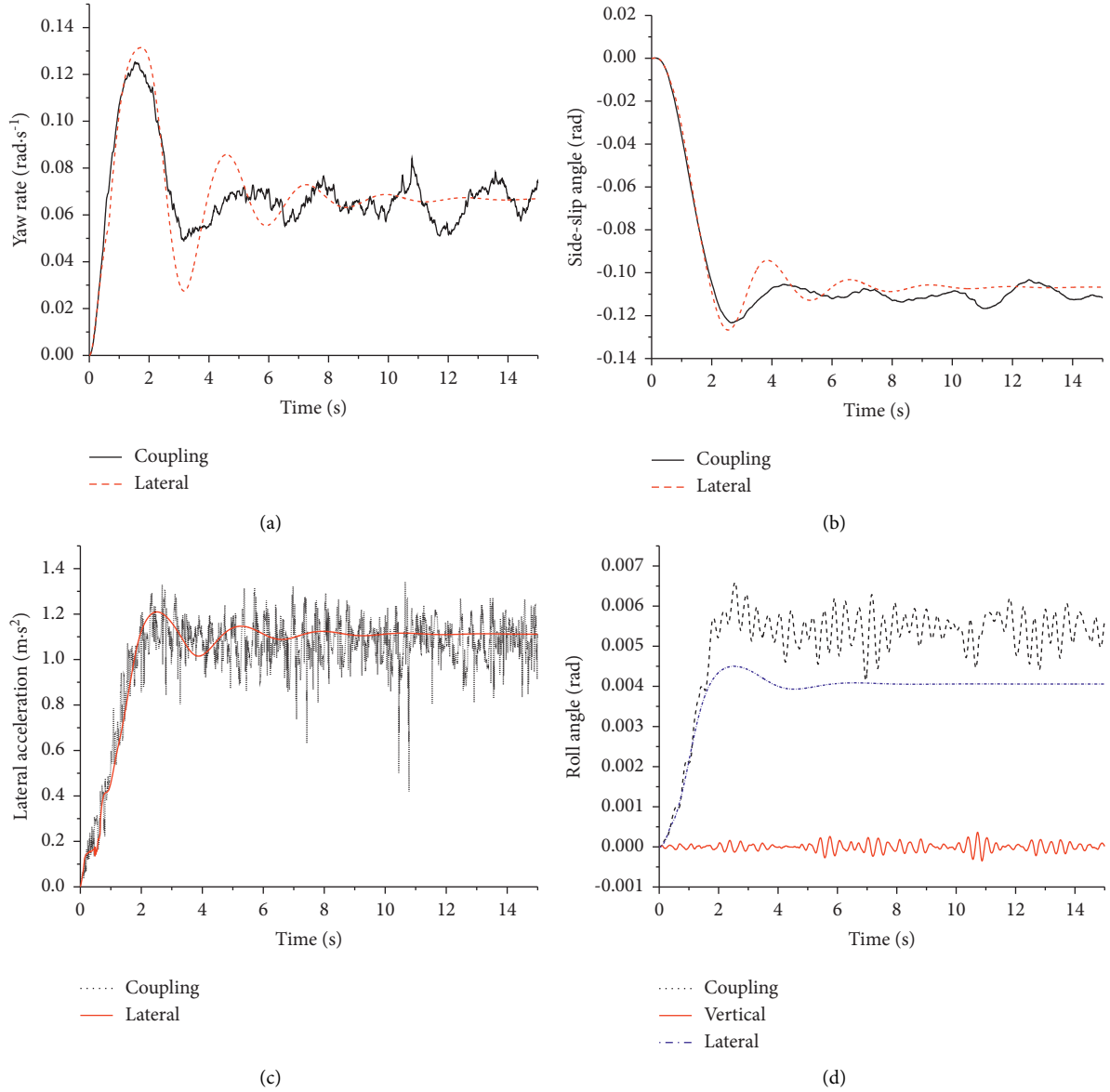
FIGURE 7: Handling stability (angular step condition, B-level random road). (a) Yaw rate. (b) Side-lip angle. (c) Lateral acceleration. (d) Roll angle.

to the above conditions, taking the state variable $X_c = [\beta_c, w_{rc}]^T$, and controlling variable $U = \delta_f$, and then, the state space equation of the ideal model of the vehicle is as shown in

$$\dot{X}_c = AX + BU, \quad (14)$$

where $A = \begin{bmatrix} 0 & 0 \\ 0 & (-1/\tau) \end{bmatrix}$, $B = \begin{bmatrix} 0 & 0 \\ 0 & (k/\tau) \end{bmatrix}$, where k and τ can be solved as equations (14) and (15):

$$k = \frac{2k_{cf}v_x(a_1 + a_2 - (a_3 - a_2)/2)}{2k_{cf}a_1(a_1 + a_2 - (a_3 - a_2)/2) + m(a_2 - (a_3 - a_2)/2)v_x^2}, \quad (15)$$

$$\tau = \frac{I_z v_x}{2k_{cf}a_1(a_1 + a_2 - (a_3 - a_2)/2) + m(a_2 - (a_3 - a_2)/2)v_x^2}. \quad (16)$$

3.2. Front Wheel Active Steering Control of Six-Wheel Active Steering.
As mentioned in the previous introduction, although there are many advanced control strategies, fuzzy
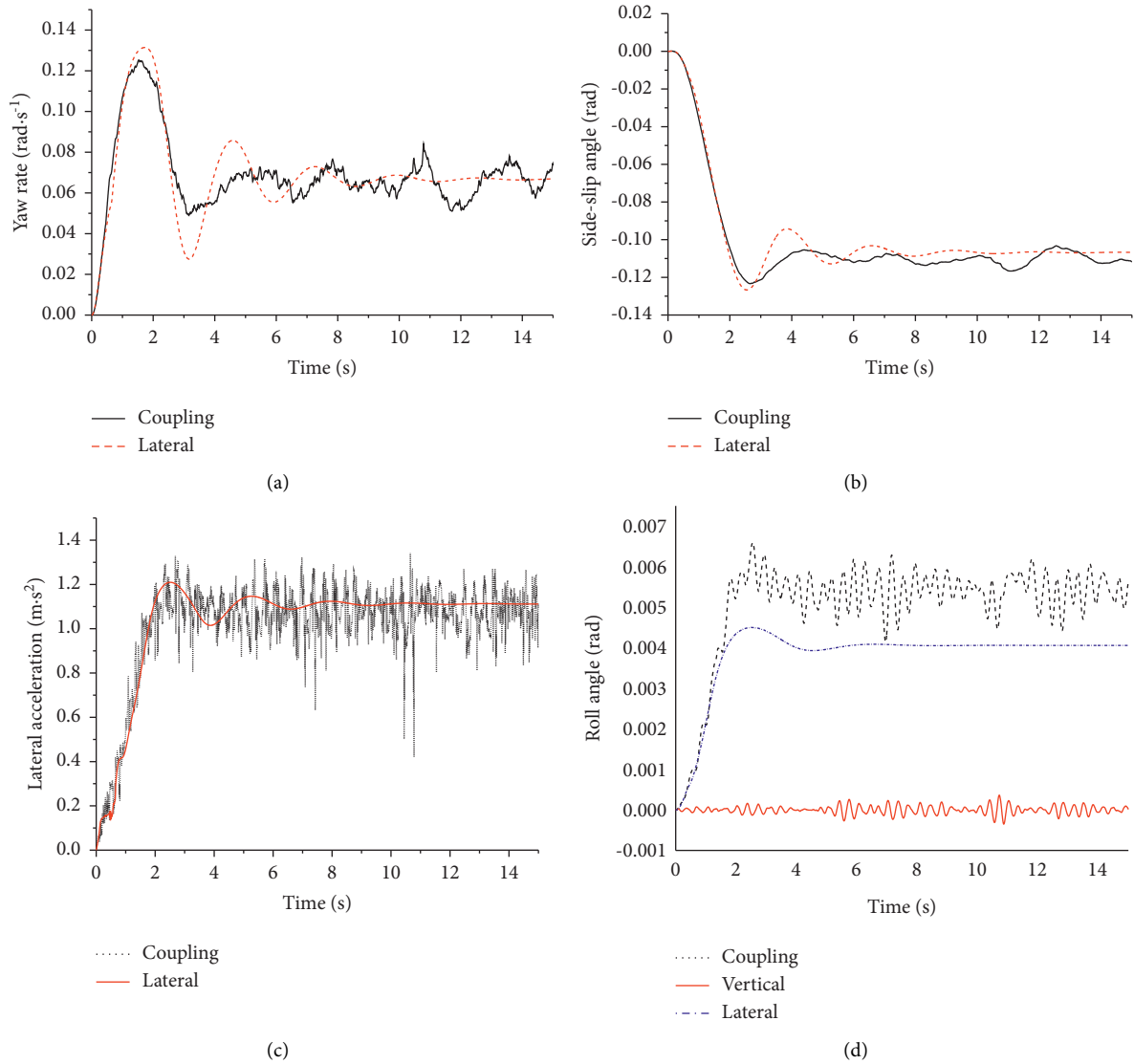
(a)

(b)

(c)

(d)

FIGURE 8: Handling stability (serpentine working condition, B-level random road). (a) Yaw rate. (b) Side-slip angle. (c) Lateral acceleration. (d) Roll angle.

PID control has the advantages of simple structure, good stability, and high reliability and is especially suitable for deterministic control systems that can establish accurate mathematical models. For the front wheel active control, a fuzzy PID controller is first designed in this section. The difference between the yaw rate of the established vehicle model and the ideal model and its rate of change are taken as the input. The ideal setting of the controller is zero, entering the additional front wheel angle output value into the vehicle model as a control amount; In the fuzzy PID controller, set the fuzzy domain of input(error of yaw rate) and its rate of change, and the fuzzy domains of output ΔK_p, ΔT_d, and ΔTi are all $[-3, 3]$, When fuzzifying, the membership function of the two inputs is Gaussian function, and the membership function of the three outputs is triangular function. The fuzzy control rules for the three parameters are also found in

reference [32]. The physical domain of the side-slip angle of the center of mass and its rate of change in error are $[-0.2, 0.2]$ and $[-0.06, 0.06]$, which are also solved by the solution formula of scale factor and quantization factor.

After obtaining the proportional coefficient k_2 of the rear axle tire and the front axle tire through the fuzzy PID controller, the ratio coefficient k_1 of the middle axle tire and the front axle tire is obtained by using a single input and single output fuzzy controller with k_2 as an input. Seven language values (negative large (NB), negative medium (NM), negative small (NS), zero (ZE), small (PS), center (PM), and Zhengda (PB)) are used to describe the relationship between k_1 and k_2, The fuzzy controller is based on the assumption that the steering of the middle and rear axles is always the same when the vehicle is being steering, to meet the relationship between the front wheel, the middle wheel,
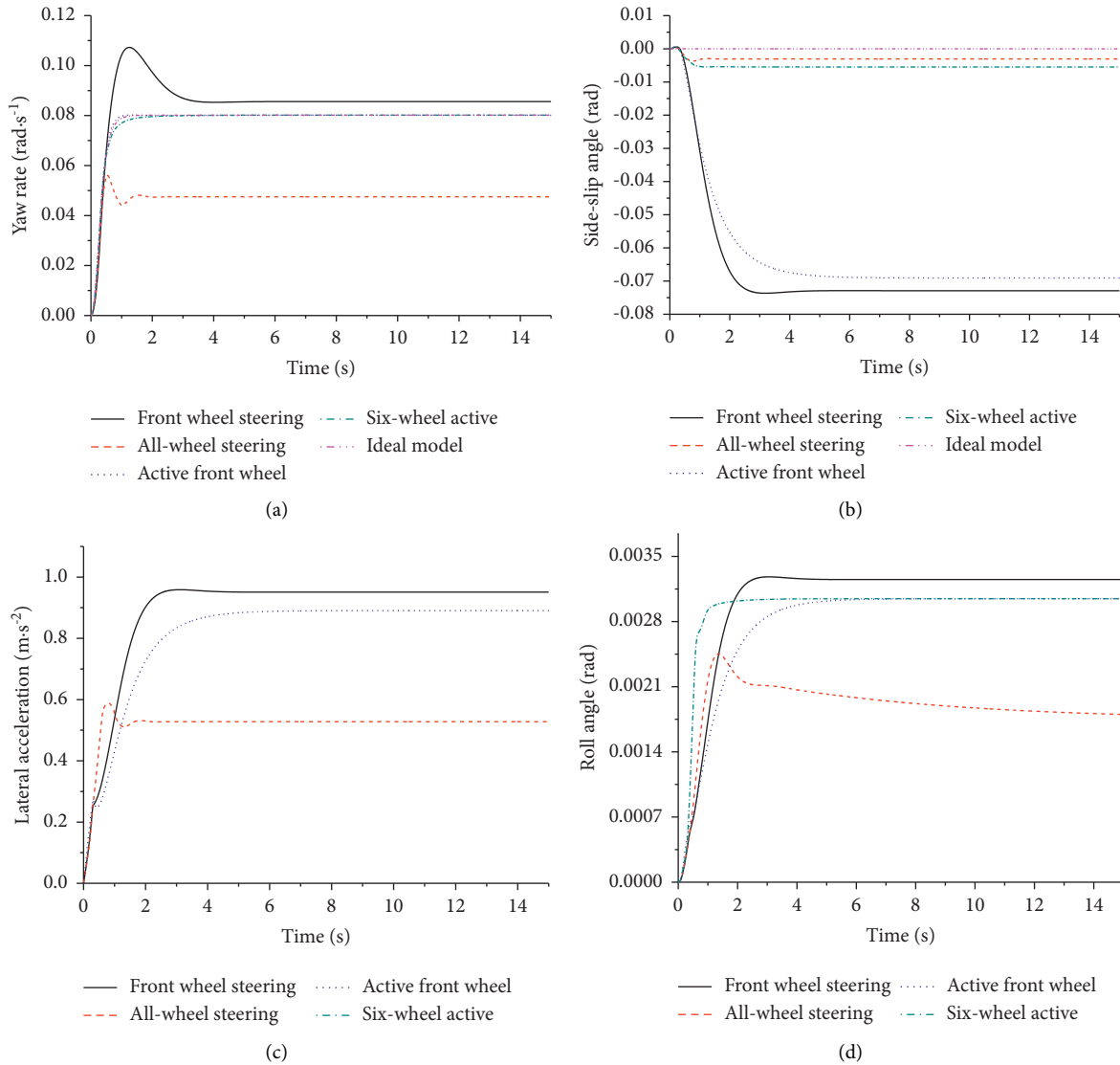
FIGURE 9: Comparison of different control strategies (40 km/h). (a) The yaw rate. (b) The side-slip angle. (c) The lateral acceleration. (d) The roll angle.

and the rear wheel angle at different speeds to ensure the safety of the vehicle. The control rules are shown in Table 2.

According to the experience, the range of the ratio of the rear axle tire to the front wheel angle is [−1, 1], the fuzzy domain of the fuzzy controller is [−1, 1], and the way of defuzzing is the centroid method.

4. Simulation Test and Result Analysis

4.1. Comparative Analysis of Dynamic Response of Coupled and Uncoupled Models. In order to prove that the presented vertical motion and lateral motion of the proposed coupling vehicle model are mutually influenced and correlated, simulation analysis is carried out. The simulation contents include (1) Angular step condition: B-level random road, and the front wheel turning angle is 0.1 rad; (2) Serpentine working condition: B-level random road. The differences

between the proposed coupled model and the independent vertical and lateral dynamic models are compared from two aspects: ride comfort and handling stability.

4.1.1. Response Comparison on Ride Comfort. The comparative analysis of responses expressing vehicle ride comfort under the vertical/lateral coupling model is shown in Figures 5 and 6.

It can be seen from Figure 5 that, under the same working conditions, the vertical acceleration, the vibration trend of the pitch angular acceleration, the vibration amplitude, and the Root Mean Square (RMS) value of the vehicle coupling model and the vertical model are almost the same. However, the vibration amplitude of the roll angular acceleration of the coupled model is significantly larger than that of the vertical
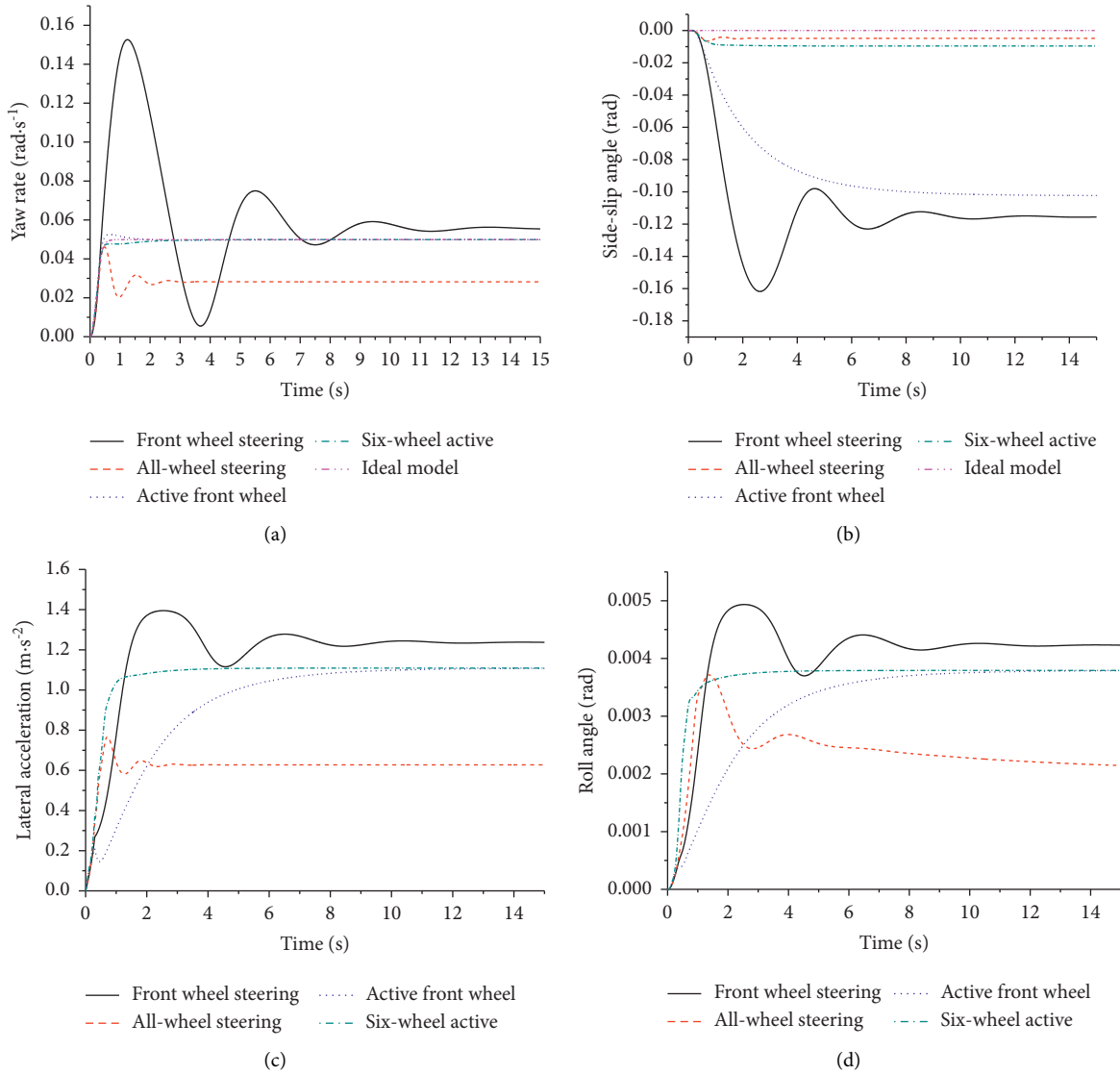
FIGURE 10: Comparison of different control strategies (80 km/h). (a) The yaw rate. (b) The side-slip angle. (c) Lateral acceleration. (d) The roll angle.

model, and the RMS values of the three working conditions differ by 64% and 77%, respectively. Therefore, a frequency domain analysis of the roll angular acceleration is performed. The amplitude of the power spectral density of the roll angular acceleration of the coupled model is also larger than that of the vertical model, especially in the medium and high frequency domains. It reflects the influence of the lateral motion of the vehicle on the vertical motion when turning.

It can be seen from Figure 6 that, with the change of the input angle of the front wheel, the curve vibration amplitudes of the three parameters of the vertical model are exactly the same as their RMS values, and the curve vibration amplitudes of the vertical acceleration and pitch acceleration of the coupled model are the same, as its RMS value is almost unchanged. However, the vibration amplitude of the curve

of the roll angular acceleration is significantly smaller, and the RMS value of the roll angular acceleration is reduced by 35% from the angular step condition to the serpentine condition. Therefore, the vehicle vertical model can only reflect the influence of the road surface grade on the vehicle ride comfort, while the vehicle coupling model can simultaneously reflect the influence of the road surface grade and the front wheel angle input on the vehicle vertical motion.

In summary, the coupled model can be obtained to evaluate the ride comfort of the vehicle more comprehensively and accurately during steering.

4.1.2. Response Comparison of Handling Stability. The comparative analysis handling stability under the vertical/ lateral coupling model is shown in Figures 7 and 8.
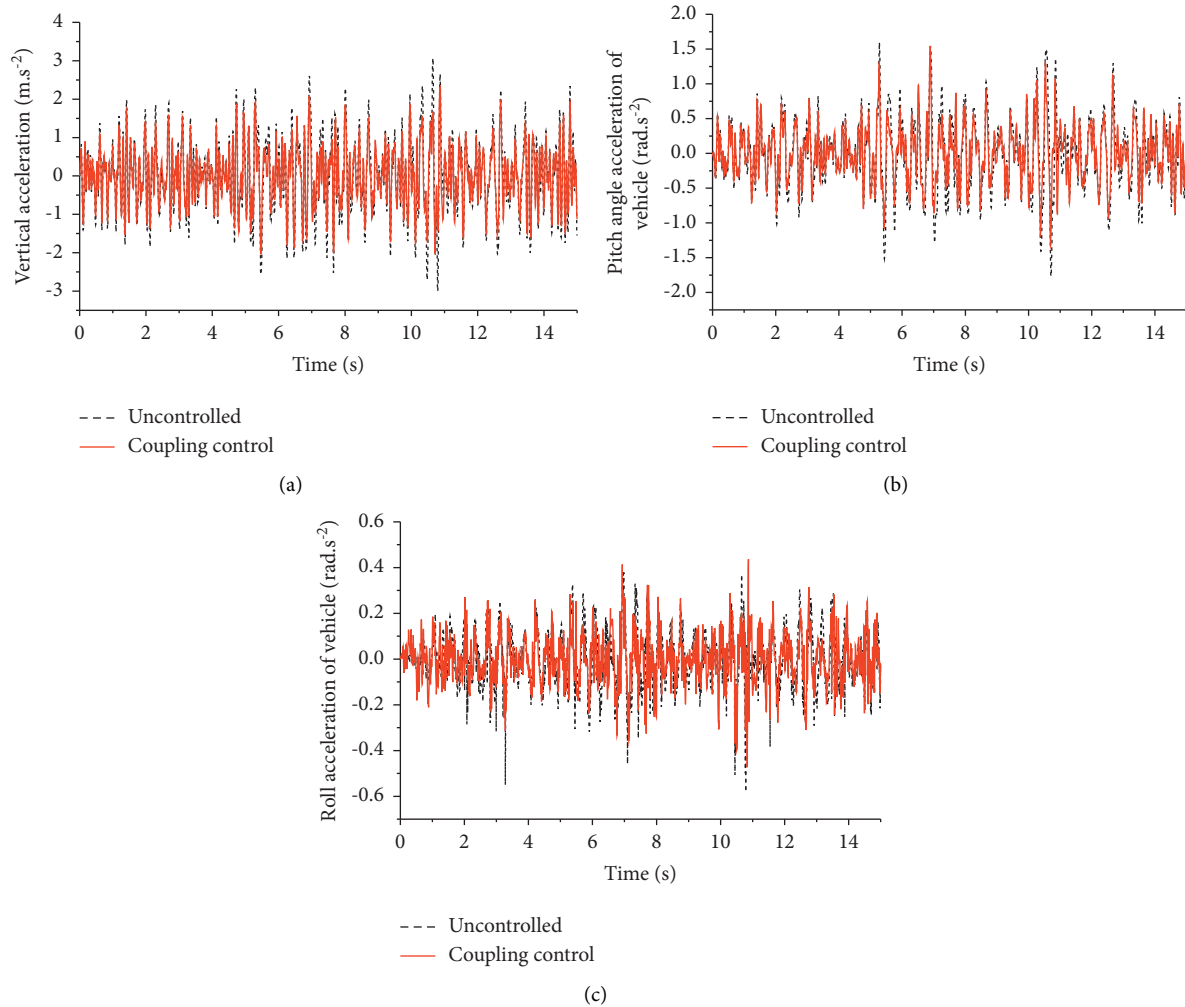
(a)

(b)

(c)

FIGURE 11: Ride comfort control result under angle step condition. (a) Vertical acceleration of vehicle. (b) Pitch angle acceleration of vehicle. (c) Roll acceleration of vehicle.

It can be seen from Figures 7 and 8 that the changes of the yaw rate, the side-slip angle of mass, the lateral acceleration, and the roll angle of the coupled model and the lateral model are roughly the same. However, each response curve of the coupled model fluctuates all the time, reflecting the influence of road unevenness on the lateral motion of the vehicle. With the change of the front wheel turning angle, the roll angle of the vertical model does not change but fluctuates around a certain value, which reflects the limitations of the vertical model.

To sum up, it is shown that the vertical motion and lateral motion of the vehicle are interrelated and inseparable from each other when steering on random uneven road surfaces. The independent vertical model cannot reflect the influence of the front wheel angle on the vehicle roll angle, roll angle acceleration, and tire vertical load and other vertical motion response quantities when the vehicle is turning. The independent lateral model cannot reflect the influence of road surface grade on vehicle lateral motion response such as vehicle tire vertical load, yaw rate, and the side-slip angle of mass. The vehicle vertical/lateral coupling model proposed in this paper makes up for these deficiencies of the independent model. It can comprehensively describe the vertical motion and lateral motion of the vehicle during steering and can simultaneously and comprehensively evaluate the ride comfort and handling stability.

4.2. Analysis of Vehicle Performance Control Effect Based on Coupling Model

4.2.1. Control Effect of Six-Wheel Active Steering Control Method. On a flat road, the speed is 40 km/h, 60 km/h, and 80 km/h, the front wheel turning angle is 0.1 rad, and the active front-wheel steering, all-wheel steering, and front-wheel steering are compared, shown in Figures 9~11.
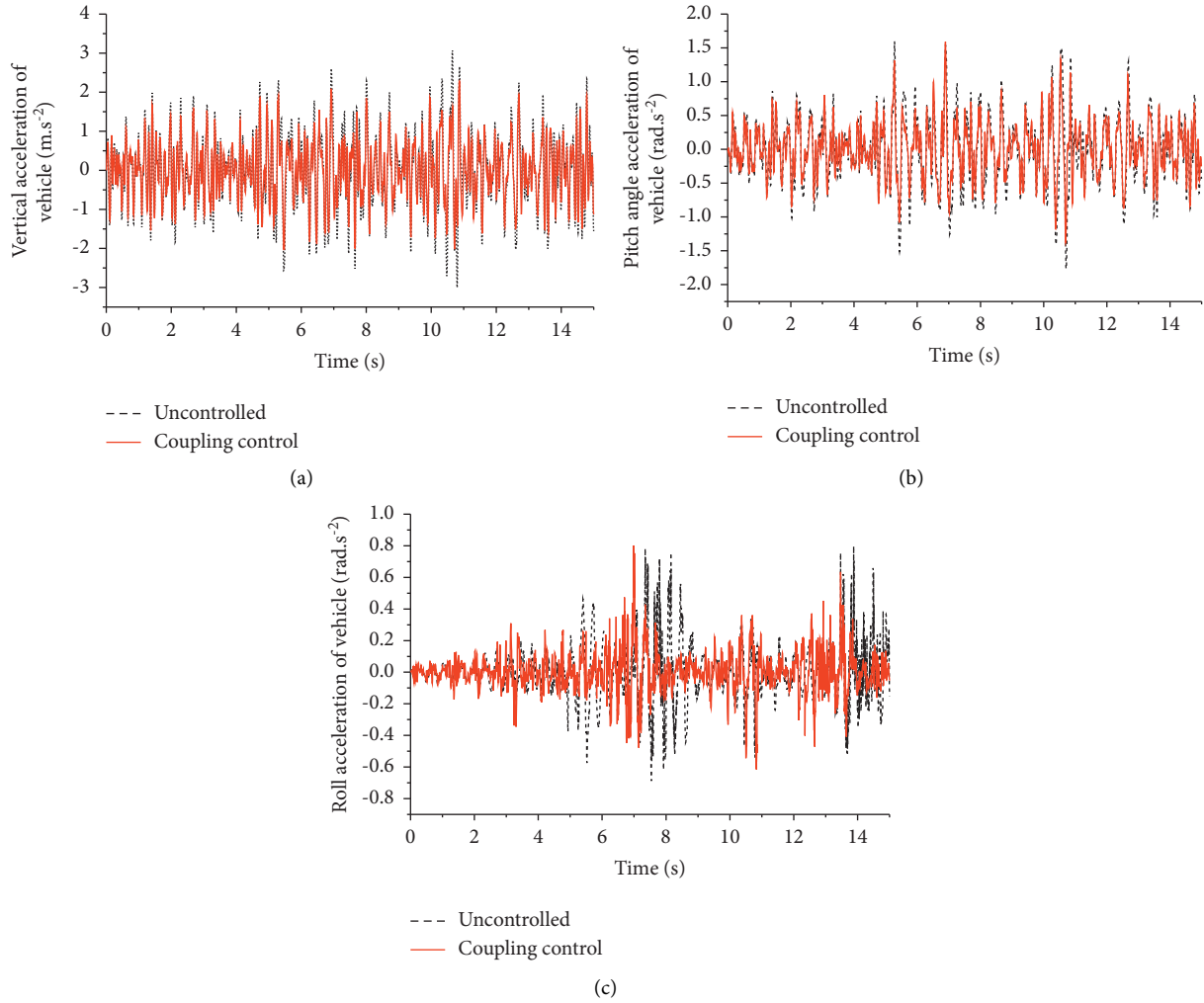
(a)

(b)

(c)

FIGURE 12: Ride comfort control result under serpentine condition. (a) Vertical acceleration of vehicle. (b) Pitch angle acceleration of vehicle. (c) Roll acceleration of vehicle.

TABLE 3: Comparison of ride comfort control (B-level road).

Working condition	Control type	Vertical acceleration of vehicle ($m \cdot s^{-2}$)	Pitch acceleration of vehicle ($rad \cdot s^{-2}$)	Roll angle acceleration of vehicle ($rad \cdot s^{-2}$)
Angular step	Uncontrolled	0.766 6	0.393 1	0.107 9
	Coupling control	0.923 3	0.494 9	0.118 7
	Improvement rate	17.0%	20.6%	9%
Serpentine	Uncontrolled	0.766 2	0.392 2	0.106 6
	Coupling control	0.923 5	0.494 9	0.170 1
	Improvement rate	17.1%	20.8%	37.3%

From Figures 8~10, we could find that the six-wheel active steering control strategy proposed in this paper can make the vehicle well track the yaw rate and the side-slip angle of the ideal model at low, medium, and high speeds. Moreover, the vehicle's side-slip angle can quickly reach a stable value, and it is extremely close to the ideal value at various vehicle speeds. The control method also has a good control effect on the lateral acceleration and body roll angle of the vehicle. Compared with the lateral acceleration and roll angle of the front-wheel steering vehicle, its response speed is faster, and the steady state value can be reached quickly. In particular, there is almost no fluctuation in the transient response.
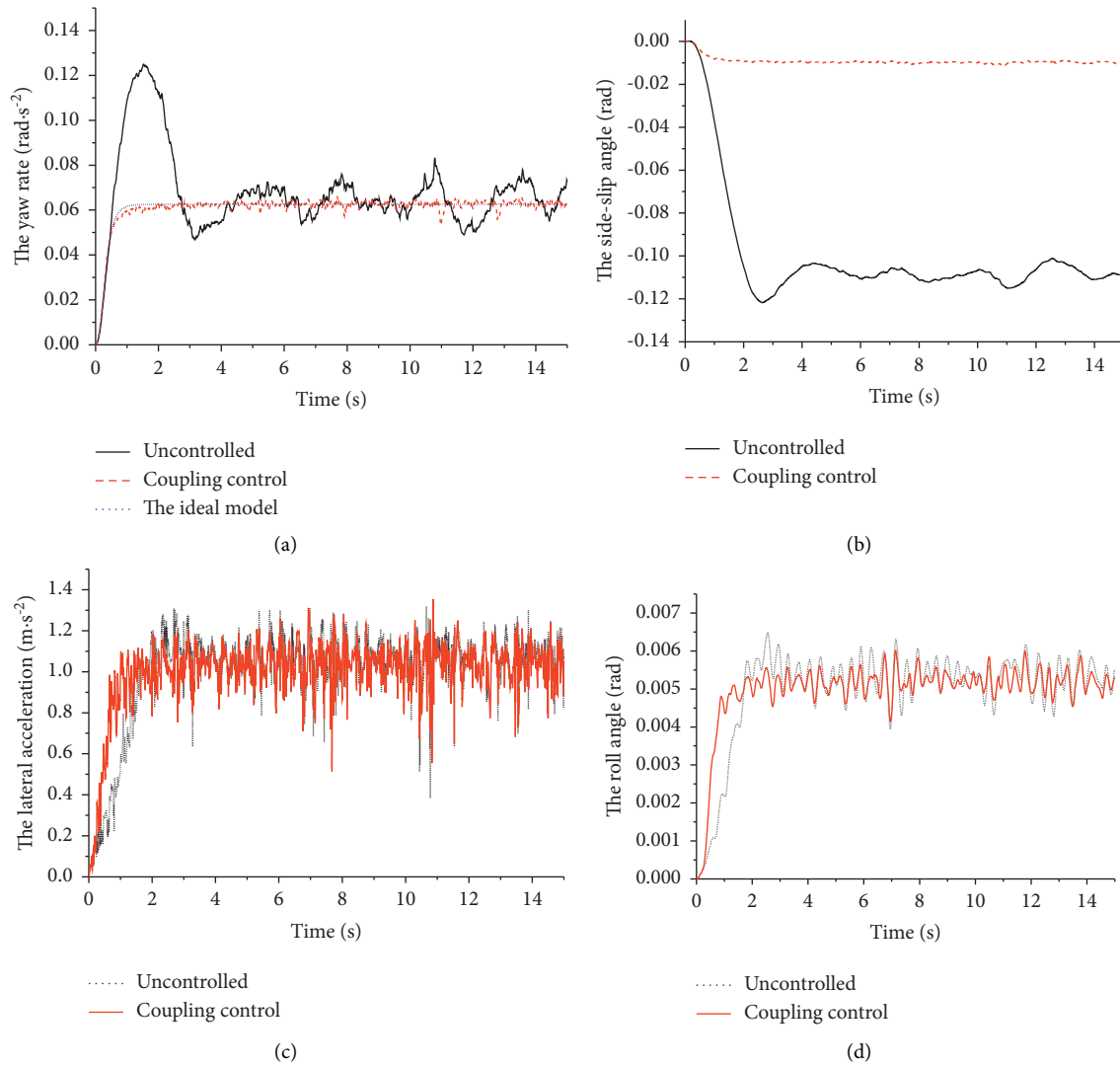
FIGURE 13: Handling stability control result under angular step. (a) Yaw rate. (b) Side-slip angle. (c) Lateral acceleration. (d) Roll angle.

4.2.2. Control Effect under the Frame of Vertical and Lateral Coupling Model. Under the same working conditions, some simulation results are compared to illustrate the improvement effect of the control method on vehicle ride comfort and steering stability. When the vehicle speed is 60 km/h, the simulation results of the main parameter control reflecting vehicle ride comfort are shown in Figures 11 and 12 under the angular step conditions and the *e* serpentine condition.

The RMS values of the main parameters reflecting the ride comfort of each working condition controlled and coupling control are shown in Table 3.

It can be seen from Figure 12 and Table 3 that the amplitude and RMS value of the vehicle body vertical acceleration, pitch angular acceleration, and roll angle acceleration are all reduced. On the same level of road, the improvement rate of the vehicle body roll angle acceleration under the serpentine condition is higher than that under the angular step condition. In general, the ride comfort of the vehicle is improved.

The control simulation results of the vehicle handling stability under the angular step conditions and the serpentine conditions are shown in Figures 13 and 14.

It can be seen from Figures 13 and 14 that, with the change of the front wheel turning angle, the control system improves the vehicle handling stability of the vertical/lateral coupling model. The motion curve of the yaw rate of the vehicle model basically coincides with the yaw rate curve of the ideal model, and the value of the side-slip angle of mass is also greatly reduced close to the ideal value of zero, which significantly reduces the risk of vehicle instability and traffic accidents. After the control, the lateral acceleration of the vehicle and the reaction time of the vehicle body roll angle are shortened, and the stable value after reaching the stable value and the vibration amplitude near the stable value are reduced.

To sum up, the control method combining semiactive suspension and six-wheel active steering can effectively reduce the main evaluation indicators of vehicle ride comfort, pitch angle acceleration, and roll angle acceleration
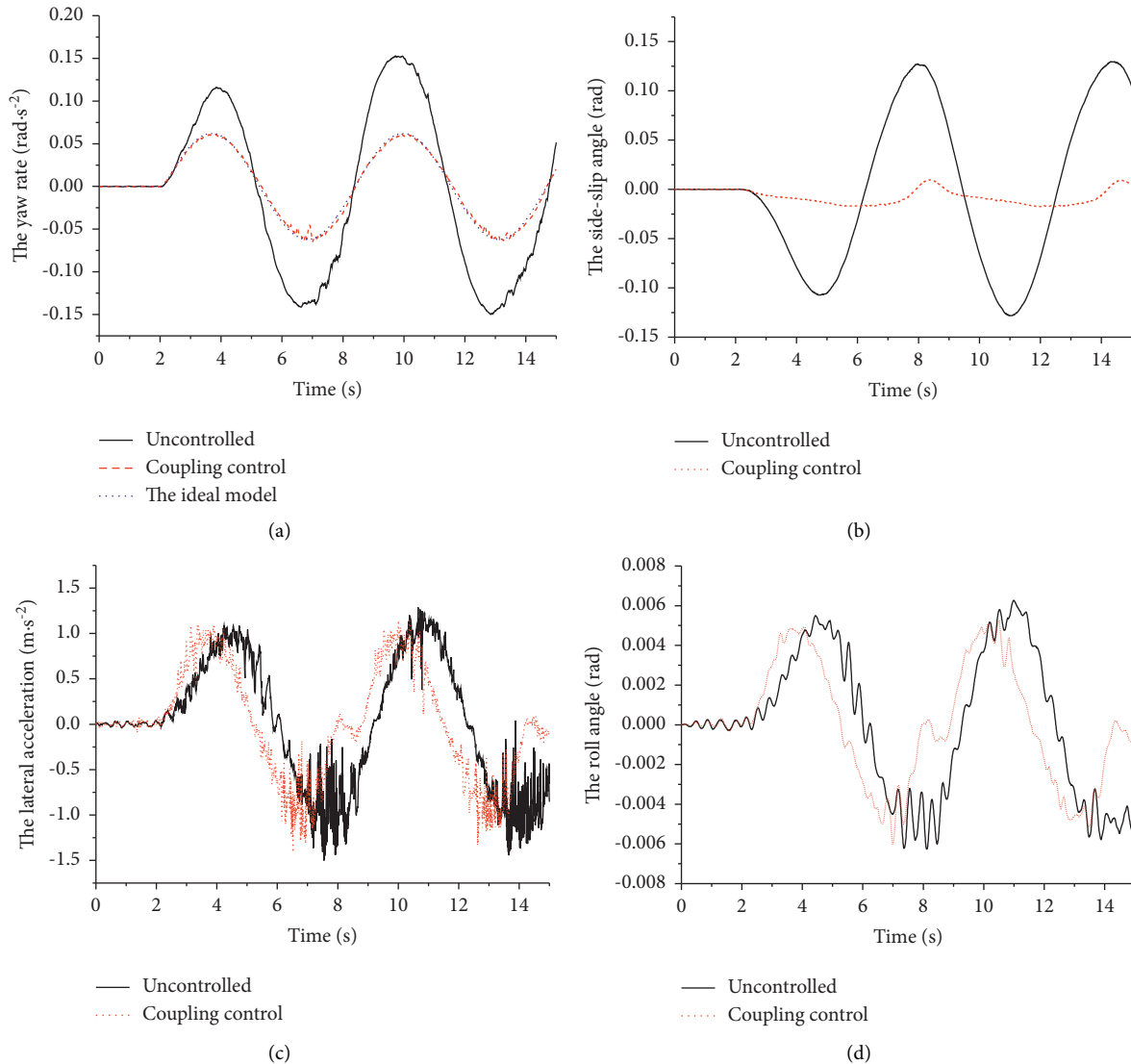
Figure 14: Handling stability control result under serpentine condition. (a) Yaw rate. (b) Side-slip angle. (c) Lateral acceleration. (d) Roll angle.

of the coupled vehicle model. The vehicle's yaw rate and centroid slip angle are close to the ideal yaw rate and centroid slip angle, and the vehicle's lateral acceleration and body roll angle are also improved.

5. Conclusions

The establishment of the vertical-lateral coupling dynamics model of the three-dimensional three-axle heavy-duty vehicle is studied. Taking the dynamic load of the tire as a link, the vertical dynamic model and the lateral dynamic model of the vehicle are coupled through the vertical motion of the tire module and the rolling motion of the vehicle body.

(1) The differences between the proposed coupling model of heavy-duty vehicle and the independent vertical and lateral dynamic models are compared from three aspects: ride comfort, tire dynamic load, and handling stability. When the vehicle is turning,

the proposed coupling model not only reflects the influence of the front wheel angle on the vertical motion and the vertical tire load, but also reflects the unevenness of the vehicle lateral motion. So, the unified dynamic model realizes the unification of vehicle dynamics models in both vertical and lateral dimensions, which is especially suitable for the turning condition of heavy vehicle.

(2) Under the framework of the vehicle vertical/lateral unified coupling dynamics model, a control system combining semiactive suspension system, six-wheel steering and front wheel active steering is established. Under the integrated control platform, the main response reflecting vehicle ride comfort and handling stability is effectively controlled. The magnitudes and RMS values of the vertical acceleration, pitch acceleration, and roll acceleration of the vehicle body after the control are reduced. The

yaw rate and the side-slip angle of the vehicle under different working conditions are obviously close to the ideal value, which avoids the instability of the vehicle under severe working conditions. The ride and handling stability of the vehicle have been simultaneously improved.

Data Availability

The multiobjective synchronous control and heavy-duty vehicles data used to support the findings of this study are included within the article.

Conflicts of Interest

The authors declare that they have no conflicts of interest.

Acknowledgments

References

[1] C. J. Kahane, *Updated Estimates of Fatality Reduction by Electronic Stability Control*, National Highway Traffic Safety Administration, Washington DC, USA, 2014.

[2] K. Yu, L. Lin, M. Alazab, L. Tan, and B. Gu, "Deep learning-based traffic safety solution for a mixture of autonomous and manual vehicles in a 5G-Enabled intelligent transportation system," *IEEE Transactions on Intelligent Transportation Systems*, vol. 22, no. 7, pp. 1–11, 2020.

[3] F. Ding, Y. Keping, Z. Gu, X. Li, and Y. Shi, "Perceptual enhancement for autonomous vehicles: restoring visually degraded images for context prediction via adversarial training," *IEEE Transactions on Intelligent Transportation Systems*, vol. 3, 2021.

[4] L. Zhang, Z. Zhang, Z. Wang, J. J. Deng, and D. G. Dorrell, "Chassis coordinated control for full X-by-wire vehicles-A review," *Chinese Journal of Mechanical Engineering*, vol. 34, no. 1, pp. 1–25, 2021.

[5] B. Zhang and Z. Li, "Mathematical modeling and nonlinear analysis of stiffness of double wishbone independent suspension," *Journal of Mechanical Science and Technology*, vol. 35, no. 12, pp. 5351–5357, 2021.

[6] A. Pazooki, S. Rakheja, and D. Cao, "Modeling and validation of off-road vehicle ride dynamics," *Mechanical Systems and Signal Processing*, vol. 28, no. 3, pp. 679–695, 2012.

[7] Z. W. Fan, Y. Wang, and C. Zhi, "Vehicle smoothness optimization analysis based on artificial fish swarm algorithm," *Journal of Agricultural Engineering*, vol. 32, no. 6, pp. 107–114, 2016.

[8] M. Ahmadian, "Magneto-rheological suspensions for improving ground vehicle's ride comfort, stability, and handling," *Vehicle System Dynamics*, vol. 55, no. 10, pp. 1618–1642, 2017.

[9] J. Jiang and A. Astolfi, "Lateral control of an autonomous vehicle," *IEEE Transactions on Intelligent Vehicles*, vol. 3, no. 2, pp. 228–237, 2018.

[10] N. Guo, B. Lenzo, X. Zhang, Y. Zou, R. Zhai, and T. Zhang, "A real-time nonlinear model predictive controller for yaw motion optimization of distributed drive electric vehicles," *IEEE Transactions on Vehicular Technology*, vol. 69, no. 5, pp. 4935–4946, 2020.

[11] N. Guo, X. Zhang, Y. Zou, B. Lenzo, G. Du, and T. Zhang, "A supervisory control strategy of distributed drive electric vehicles for coordinating handling, lateral stability, and energy efficiency," *IEEE Transactions on Transportation Electrification*, vol. 7, no. 4, pp. 2488–2504, 2021.

[12] A. Norouzi, M. Masoumi, A. Barari, and S. S. Farrokhpour, "Lateral control of an autonomous vehicle using integrated backstepping and sliding mode controller," *Proceedings of the Institution of Mechanical Engineers - Part K: Journal of Multibody Dynamics*, vol. 233, no. 1, pp. 141–151, 2019.

[13] X. Zhang, P. Wang, J. Lin, H. Chen, J. Hong, and L. Zhang, "Real-Time nonlinear predictive controller design for drive-by-wire vehicle lateral stability with dynamic boundary conditions," *Fundamental Research*, vol. 2, no. 1, pp. 131–143, 2022.

[14] H. Bu, A. Li, X. Huang, W. Li, and J. Wang, "Optimal design of the six-wheel steering system with multiple steering modes," *Mathematical Problems in Engineering*, vol. 2021, Article ID 1716116, 18 pages, 2021.

[15] Y. X. Li, Y. C. Wang, and P. F. Feng, "Lateral dynamics of three-axle steering vehicle based zero vehicle sideslip angle control," *Advanced Materials Research*, vol. 476, pp. 1682–1687, 2012.

[16] W. Liu, H. He, F. Sun, and J. Lv, "Integrated chassis control for a three-axle electric bus with distributed driving motors and active rear steering system," *Vehicle System Dynamics*, vol. 55, no. 5, pp. 601–625, 2017.

[17] H. A. Khan, S. N. Yun, E. A. Jeong, J. W. Park, C. M. Yoo, and S. M. Han, "A review of rear axle steering System technology for commercial vehicles," *Journal of Drive and Control*, vol. 17, no. 4, pp. 152–159, 2020.

[18] H. Wang, Q. Wang, W. Chen, L. Zhao, and D. Tan, "A novel path tracking approach considering safety of the intended functionality for autonomous vehicles," *Proceedings of the Institution of Mechanical Engineers - Part D: Journal of Automobile Engineering*, vol. 236, no. 4, pp. 738–752, 2021.

[19] J. .. Sun, J. Cong, W. Zhao, and Y. Zhang, "Actuator fault-based integrated control for vehicle chassis system," *Measurement and Control*, vol. 54, no. 1-2, pp. 25–43, 2021.

[20] J. Yao, G. Lv, M. Qv, Z. Li, S. Ren, and S. Taheri, "Lateral stability control based on the roll moment distribution using a semiactive suspension," *Proceedings of the Institution of Mechanical Engineers - Part D: Journal of Automobile Engineering*, vol. 231, no. 12, pp. 1627–1639, 2017.

[21] R. Jiang and D. Wang, *Optimization of Vehicle Ride comfort and Handling Stability Based on TOPSIS Method*, SAE Technical Paper, PA, USA, 2015.

[22] Y. Cheng, W. Shi, W. Liu, and G. H. Sun, "Optimization of ride comfort and handing stability base on virtual prototyping," in *Proceedings of the Seventh International Conference on Natural Computation*, pp. 803–806, Shanghai China, July 2011.

[23] J. Sun, J. Cong, L. Gu, and M. Dong, "Fault-tolerant control for vehicle with vertical and lateral dynamics," *Proceedings of the Institution of Mechanical Engineers - Part D: Journal of Automobile Engineering*, vol. 233, no. 12, pp. 3165–3184, 2019.

[24] S. Fergani, L. Menhour, O. Sename, L. Dugard, and B. D. Novel, "Integrated vehicle control through the coordination of longitudinal/lateral and vertical dynamics controllers: flatness and LPV/H∞-based design," *International*

Journal of Robust and Nonlinear Control, vol. 27, no. 18, pp. 4992–5007, 2017.

[25] H. Zhao, W. Chen, J. Zhao, Y. Zhang, and H. Chen, "Modular integrated longitudinal, lateral, and vertical vehicle stability control for distributed electric vehicles," *IEEE Transactions on Vehicular Technology*, vol. 68, no. 2, pp. 1327–1338, 2019.

[26] K. Kwon, M. Seo, H. Kim, T. H. Lee, J. Lee, and S. Min, "Multi-objective optimisation of hydro-pneumatic suspension with gas-oil emulsion for heavy-duty vehicles," *Vehicle System Dynamics*, vol. 58, no. 7, pp. 1146–1165, 2020.

[27] K. Huh, J. Kim, and J. Hong, "Handling and driving characteristics for six-wheeled vehicles," *Proceedings of the Institution of Mechanical Engineers - Part D: Journal of Automobile Engineering*, vol. 214, no. 2, pp. 159–170, 2000.

[28] L. Chen, P. Li, W. Lin, and Q. Zhou, "Observer-based fuzzy control for four-wheel independently driven electric vehicles with active steering systems," *International Journal of Fuzzy Systems*, vol. 22, no. 1, pp. 89–100, 2020.

[29] S. V. Nikzad and M. Naraghi, *Model reference tracking control a 4WS vehicle using single and dual steering strategies*, SAE Paper, PA, USA, 2002.

[30] A. V. Alagappan, K. N. N. Rao, and R. K. Kumar, "A comparison of various algorithms to extract Magic Formula tyre model coefficients for vehicle dynamics simulations," *Vehicle System Dynamics*, vol. 53, no. 2, pp. 154–178, 2015.

[31] R. Liu, M. Wei, and W. Zhao, "Trajectory tracking control of four wheel steering under high speed emergency obstacle avoidance," *International Journal of Vehicle Design*, vol. 77, no. 1-2, p. 1, 2018.

[32] L. Yuan, W. P. Liu, and X. X. Liu, "Design of sliding mode controller for all-wheel steering system of three-axle vehicle," *Acta Armamentarii*, vol. 36, no. 8, pp. 1391–1397, 2015.

[33] G. Zeng, J. Hu, D. Wang, and L. Chungling, *Fuzzy Control Theory and Engineering Application*, pp. 65-66, Wuhan: Huazhong University of Science and Technology Press, Wuhan, China, 2006.